A robust vertical nanoscaffold for recyclable, paintable, and flexible light-emitting devices

Yifan Yao, Yusheng Chen, Kuidong Wang, Nicholas Turetta, Stefania Vitale, Bin Han, Hanlin Wang, Lei Zhang, Paolo Samorì

MATERIALS SCIENCE

A robust vertical nanoscaffold for recyclable, paintable, and flexible light-emitting devices

Yifan Yao[1], Yusheng Chen[1], Kuidong Wang[1], Nicholas Turetta[1], Stefania Vitale[1], Bin Han[1], Hanlin Wang[1], Lei Zhang[2], Paolo Samorì[1]*

Organic light-emitting devices are key components for emerging opto- and nanoelectronics applications including health monitoring and smart displays. Here, we report a foldable inverted polymer light-emitting diode (iPLED) based on a self-suspended asymmetrical vertical nanoscaffold replacing the conventional sandwich-like structured LEDs. Our empty vertical-yet-open nanoscaffold exhibits excellent mechanical robustness, proven by unaltered leakage current when applying 1000 cycles of 40-kilopascal pressure loading/unloading, sonication, and folding, with the corresponding iPLEDs displaying a brightness as high as 2300 candela per square meter. By using photolithography and brush painting, arbitrary emitting patterns can be generated via a noninvasive and mask-free process with individual pixel resolution of 10 μm. Our vertical nanoscaffold iPLED can be supported on flexible polyimide foils and be recycled multiple times by washing and refilling with a different conjugated polymer capable of emitting light of different color. This technology combines the traits required for the next generation of high-resolution flexible displays and multifunctional optoelectronics.

INTRODUCTION

During the last two decades, a notable research effort has been devoted to the development of high-performance organic light-emitting materials and devices to address the technological needs in the rapidly expanding flexible electronics consumer market (*1*–*4*). In 2021, the global organic light-emitting diode (OLED)–based display market was valued at 38.4 billion dollars, with a projected increase to 72.8 billion dollars by 2026 (*5*). Phosphorescent materials, as the most commonly used second-generation organic light-emitting materials, are significantly more efficient than standard fluorescent materials in terms of luminescence when heavy metal (iridium, platinum, europium, and osmium) elements are introduced (*6*, *7*). However, the high cost and limited availability of these precious components represent major disadvantages in view of the short lifetime and the large market of OLEDs. Furthermore, in conventional OLEDs, the use of transparent indium tin oxide (ITO) as anode is indispensable as it combines high transparency, high work function (WF), and good conductivity. Nevertheless, because of its intrinsic brittleness, high processing temperature, and shortage of indium, new materials are intensively being explored to replace ITO electrodes especially in flexible devices (*8*). In this framework graphene, carbon nanotubes, metal nanowires, and conductive polymers have been studied as alternative electrode materials, yet they revealed some major drawbacks. While carbon-based electrodes do not exhibit sufficient electrical performances especially for application in large-area devices (*9*), the inherent roughness of metal nanowire– and carbon nanotube–based films determines a considerable electrical leakage when exploited as electrodes in electronic devices (*8*). On the other hand, a conventional sandwich-structured OLED is made up of a stack of organic and inorganic layers, each one having a distinct complex refraction index, resulting in a weak microcavity. As a result, 70 to 80% of the generated photons are trapped in the active organic layers and transparent ITO due to the large difference in the refractive indices *n* between the light-emitting layer and the glass substrate (*10*–*13*).

Here, we report a vertical-channel nanoscaffold for inverted polymer LEDs (iPLEDs) that is devoid of ITO. The vertical nanoscaffold is made up of millions of honeycomb-shaped nanomesh electrodes assembled in a hexagonal array supported by thousands of individual polyimide (PI) nanopyramids having a height below 260 nm. To promote charge injection and transport, asymmetric top anode and bottom cathode electrodes have been exploited. The nanoscaffold-based devices have shown high reliability and structural stability as they tolerate hard pressing, sonication, and folding. We have focused our attention on super yellow (SY) and poly(9,9-dioctylfluorene-alt-benzothiadiazole) (F8BT) as the model system for iPLEDs. The nanopores in the nanoscaffold emit light with a luminance of 2300 cd/m^2 and an external quantum efficiency (EQE) of 0.2%. Moreover, as a solid and sustainable platform, the nanoscaffold iPLEDs can be recycled after being used by washing away the embedded light-emitting materials and being reused upon hosting a different emitting polymer. The previously used light-emitting materials can be recuperated, thanks to the outstanding mechanical and structural stability of the nanoscaffold. Last, gold nanomesh, semiconducting polymers, and PI nanopyramids can be combined to develop fully functional iPLED arrays on flexible PI foil supports, which can be used as free-standing foils or as conforming layers onto arbitrary surfaces for technological applications as emissive panel or multifunctional lightening.

RESULTS

Fabrication and characterization of asymmetric vertical nanoscaffolds

Nanosphere lithography, a patterning technique that uses a hexagonal close-packed (hcp) nanosphere monolayer as a mask, enables the generation of standard honeycomb-shaped nanomesh (*14*, *15*). First, a 40-nm Al film was evaporated onto a glass substrate through a mask as the bottom electrode. The electron transport layer zinc

[1]Université de Strasbourg, CNRS, ISIS UMR 7006, 8 allée Gaspard Monge, F-67000 Strasbourg, France. [2]Key Laboratory of Mesoscopic Chemistry of MOE, School of Chemistry and Chemical Engineering, Nanjing University, Nanjing, Jiangsu 210023, China.
*Corresponding author. Email: samori@unistra.fr

oxide (ZnO) was then prepared by the reorganization of gel particles of zinc acetate dihydrate [$Zn(CH_3COO)_2\ 2H_2O$] (*16*, *17*). Intermittent contact atomic force microscope (AFM) imaging confirmed that the ZnO film has a thickness around 36 nm and a notable flatness as attested by a room mean square roughness (R_{RMS}) of 1.06 nm estimated on an area of 5 μm by 5 μm (fig. S1). Subsequently, a PI dielectric layer was spin-coated onto the substrate exposing prepatterned ZnO/Al bottom electrodes (Fig. 1A and fig. S2). Before self-assembly of the polystyrene (PS) nanospheres into an hcp monolayer, an ultra-thin chromium (Cr) layer (thickness = 0.8 nm) was vacuum sublimed on top of PI before oxygen plasma treatment to protect it from getting damaged. The 800-nm PS nanospheres were then deposited onto the surface, and the spacing between adjacent PS nanospheres was enhanced via oxygen plasma treatment (fig. S3). The nanomesh electrode was patterned by evaporating a thin layer of gold (40 nm) through the PS nanosphere mask, followed by the liftoff process (diameter of the nanopores: ~680 nm) (*18*). Last, to obtain the vertical-yet-open nanoscaffold, Cr etchant was used to remove the 0.8-nm Cr protective layer, and an oxygen plasma treatment was used to etch away PI. Because of the transverse drilling effect, the PI underneath the nanomesh electrode was also etched away. By controlling the duration of the oxygen plasma etching, regularly aligned PI nanopyramids were shaped to support the Au nanomesh by preventing it from collapsing onto the bottom electrode (Fig. 1B). For the final device, the exposed bottom surface of ZnO/Al was designed to act as the cathode, while the top Au nanomesh operates as the anode.

Figure 1C shows a photograph of the resulting patterned vertical nanoscaffold devices. The polychromatic shades originate from the light dispersion effects of the nanopores with a periodic arrangement comparable to the wavelength of visible light. To better illustrate the device topology of the vertical nanoscaffold iPLEDs, a three-dimensional (3D) cartoon and corresponding 2D cross-sectional perspective are displayed in Fig. 1 (D and E). The iPLEDs were made via the sequential deposition of ethanolamine (EA), SY/F8BT, and poly(methyl methacrylate) (PMMA) onto the bare nanoscaffold, as described in detail in Materials and Methods. Figure 1E illustrates the entire device structure and cross-sectional view of the nanoscaffold-based iPLED, which includes the cathode (aluminum), electron transport layer (ZnO), electron injection layer (EA), dielectric spacer layer (PI nanopyramids), light-emitting layer (SY/F8BT), nanomesh anode (gold), and encapsulation layer (PMMA), respectively.

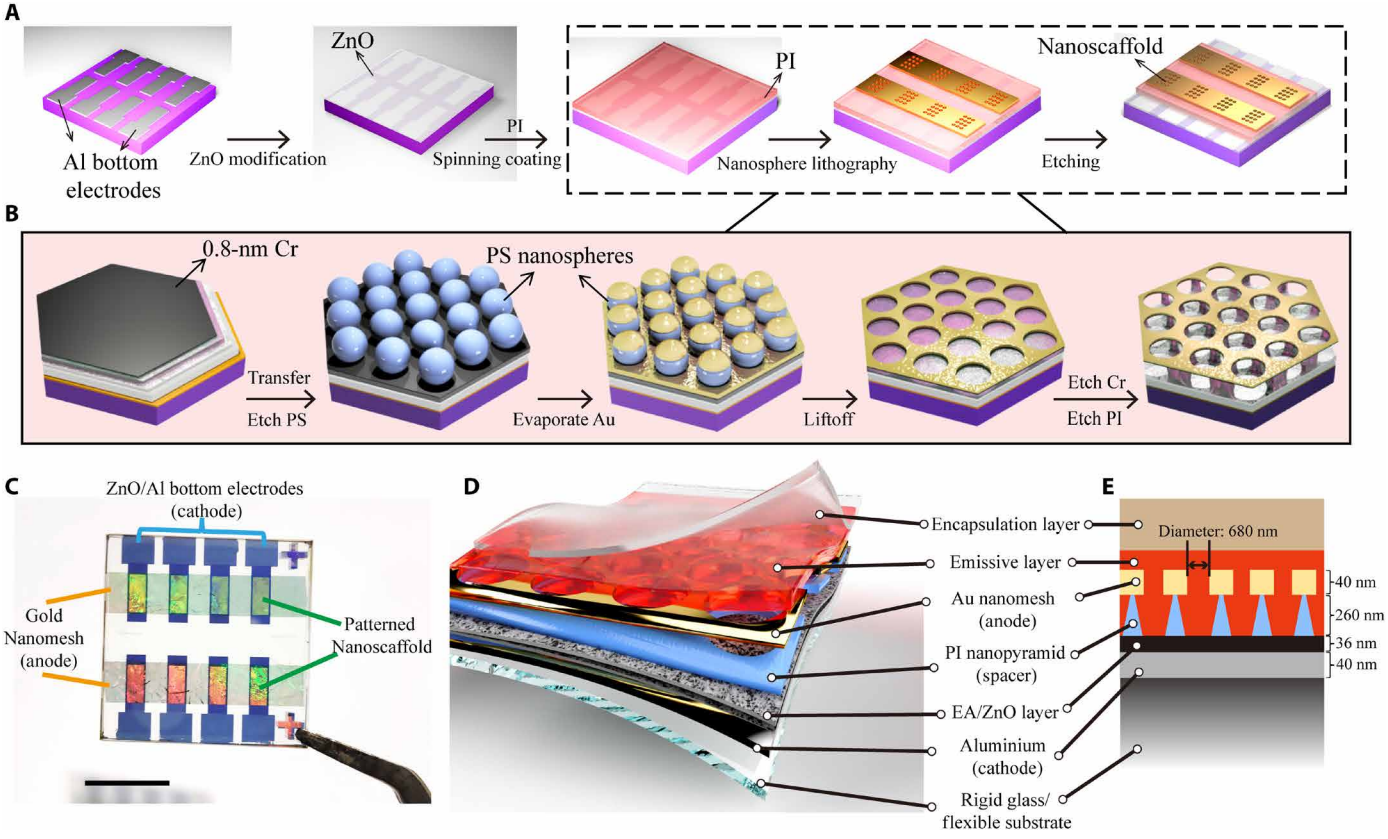

Fig. 1. The fabrication scheme of asymmetric vertical nanoscaffold. (**A**) Fabrication procedure for the vertical-yet-open nanoscaffold array through nanosphere lithography. ZnO sol-gel was spin-coated on aluminum electrodes and thermally annealed in air. PI was deposited onto a ZnO/Al substrate. After the gold nanomesh electrodes were patterned by using nanosphere lithography, the PI layer was removed with an oxygen plasma etching, resulting in nanopyramid-shaped spacers to support the gold nanomesh electrode. (**B**) The detailed vertical nanoscaffold fabrication procedure. A thin barrier layer of Cr (0.8 nm) was vacuum-deposited on top of the PI layer: The transferred monolayer of PS nanospheres was etched by O_2 plasma. The nanomesh electrode was then patterned by evaporating a thin layer of gold through the PS nanosphere mask, followed by the liftoff process. As the last step, the nanopyramid-supported nanomesh electrode was formed by oxygen plasma etching through the PI layer. (**C**) The final patterned nanoscaffold devices. (**D**) Cartoon depicting the device architectures of iPLEDs realized by the vertical nanoscaffold. (**E**) Corresponding schematic cross section (front view) of iPLEDs based on vertical nanoscaffold.

The self-suspended vertical nanoscaffold can reach a high degree of structural uniformity over hundreds of micrometers square due to the ability of PS nanospheres to self-assemble into hcp monolayers (Fig. 2A). Figure 2B shows that the nanopyramid-shaped PI spacers are robust and vertically aligned, supporting the 40-nm gold nanomesh by preventing their collapse or folding, as revealed by scanning electron microscopy (SEM) images recorded with a tilt angle of 40°. The exposed bottom surface of ZnO/Al was designed to operate as the cathode electrode, with the interelectrodic distance in our device being therefore determined by the thickness of PI nanopyramid spacers (~260 nm; Fig. 2C). Different interelectrodic distances were studied to assess the influence of dielectric layer thickness (figs. S4 and S5). As expected, a larger background leakage current density was detected when a thinner PI layer (120 nm) was used (fig. S4, C and D). When the PI layer thickness exceeds 200 nm, however, the background leakage current density only slightly changes upon increasing the thickness. We have therefore chosen to use the 260-nm PI layer in our experiments to lower the device's operating voltage. Figure S6 summarizes the results of a large statistical analysis of background leakage current density with 260-nm PI under DC bias. A background leakage current density below 10^{-4} mA/cm^2 at ±1.5 V was defined as an indicator of successful fabrication. Significantly, when supported on a glass substrate, 96% of the ~400 devices with an active device area of 8 mm^2 comply with such a threshold value. Since even a small local defect/collapse of the nanostructures could cause the device to short circuit, the successful construction of a large-area vertical nanoscaffold constitutes a key achievement in the field of nanotechnology.

Figure S7 shows the topography and the corresponding Kelvin probe force microscopy (KPFM) image of vertical-yet-open nanoscaffold without EA modification. The KPFM image and the surface potential (SP) profile indicated by a black straight line (fig. S7B) demonstrates that ZnO regions are characterized by a lower WF when compared to the one of the gold nanomesh (~100 mV). After spin coating a thin EA electron injection layer, the WF of both gold and ZnO is reduced by approximately the same amount, as the SP difference between the two materials is still around 100 mV (Fig. 2D and fig. S8). In our devices, this scenario is beneficial for efficient electron injection (*19*).

The vertical nanoscaffold exhibits a notably high mechanical and electrical stability. The PI nanopyramids are strong enough to hold a centimeter-sized nanomesh without collapsing (Fig. 2, A and B), with a leakage current density below 10^{-4} mA/cm^2 at ±1.5 V. To test the robustness of the nanoscaffold, a mechanical test was carried out, consisting in the cyclic application of 4- and 40-kPa pressure for a total of 1000 cycles. AFM and SEM images provided insight into the thickness and morphology of PI nanopyramids and revealed that the nanoscaffold remained intact (fig. S9). Also, current measurements after such harsh test revealed that the background leakage current density is unchanged (Fig. 2E). Significantly, SEM and AFM imaging (fig. S10) demonstrated that even the use of ultrasonic cleaning did not alter for the structure of the nanoscaffold, with no evidence of collapse or crack. Ten minutes of sonication in toluene resulted in a slightly greater background leakage current density yet still remaining acceptable and far below the 10^{-4} mA/cm^2 limitation (Fig. 2F). All these results give clear evidence that the nanopyramid-supported nanomesh electrode has exceptional structural and mechanical robustness, thus considerably expanding its practical applications.

Fabrication and theoretical modeling of vertical nanoscaffold iPLEDs

Our nanoscaffold was used to host solution-processed light-emitting materials. The light-emitting devices were fabricated in an inverted

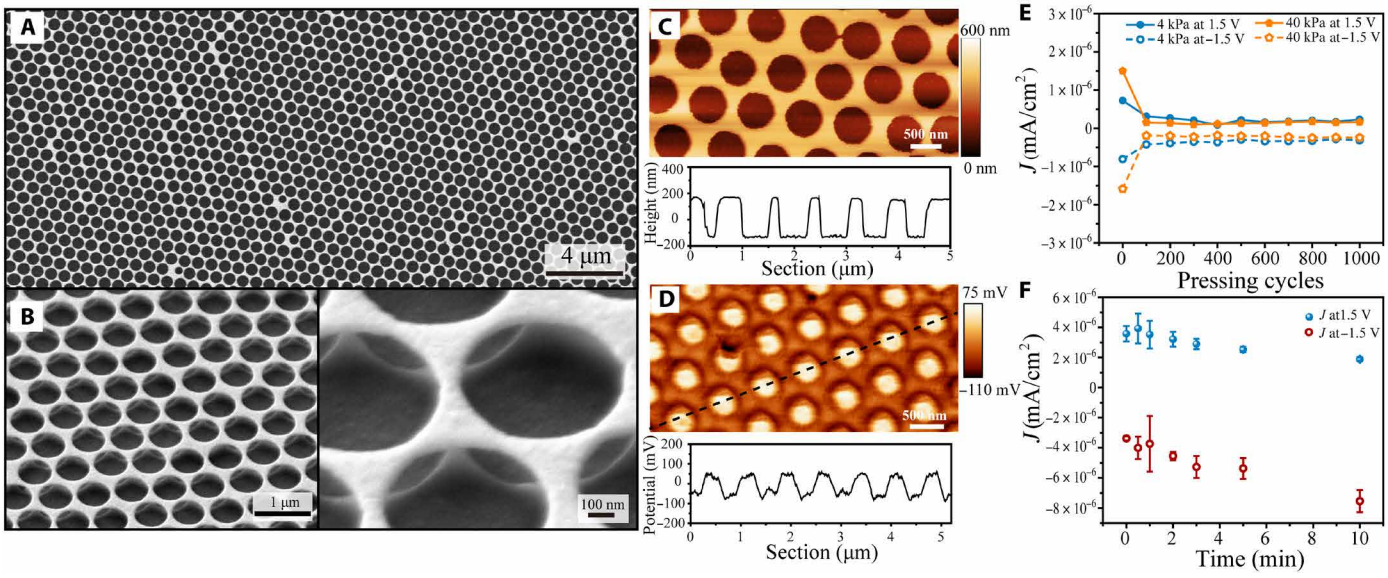

Fig. 2. The mechanical and electrical robustness of vertical nanoscaffold. (**A**) SEM image of an empty vertical nanoscaffold. (**B**) Zoom-in SEM images of the nanomesh electrode supported by PI nanopyramids (spacer) in (A) (substrate tilt angle = 40°). (**C**) Height AFM image of the vertical nanoscaffold with its topographical profile (PI: ~260 nm; gold: ~40 nm). (**D**) KPFM image of a vertical-yet-open nanoscaffold after EA modification. The bright circular features are ascribed to the bottom ZnO/Al surface, whereas the surrounding dark regions are attributed to the top gold nanomesh electrode. The bottom demonstrates a potential profile along the path indicated with a black dashed line on the image. (**E**) Background leakage current density of the empty vertical nanoscaffold before and after 1000 times of pressing. (**F**) Leakage current density of the empty vertical nanoscaffold before and after 10 min of ultrasonic cleaning in toluene. The *J-V* curves were measured in the nitrogen box by scanning the voltage from +2 to −2 V. Then, the current density at ±1.5 V is selected.

configuration, with the bottom cathode electrode being aluminum/ZnO and the top anode being the gold nanomesh (Fig. 1, D and E). An interfacial layer of EA was spin-coated into the nanopores to promote electron injection. Despite the fact that EA reduced the WF of gold nanoscaffold from 5.3 to 4.3 eV, electron extraction can be improved by lowering electron and hole recombination (fig. S11) (*17*). The light-emitting polymers (SY/F8BT) were then spin-coated and thermally annealed at 170°C to leverage their optoelectronic properties (*20*, *21*). The height of PI nanopyramids determines the thickness of the light-emitting layer. Last, PMMA was used to encapsulate the devices. The morphology of the deposited light-emitting polymer/nanoscaffold and the encapsulated device was investigated by AFM (fig. S12). As shown in fig. S12A, the corrugated light-emitting layer induced by the vertical-yet-open nanoscaffold can exhibit efficient light extraction (*22*). The quality of the films is critical in conventional sandwich stacked OLEDs, with defects or pinholes in the film causing short circuits or failures of the device, being particularly problematic in inkjet-printed devices because the films are typically not uniform. However, since the PI nanopyramids have completely separated the cathode and anode in the vertical architecture, the device can still work even if the light-emitting layer is discontinuous or comprises pinholes.

Figure 3 shows the device characterizations of the nanoscaffold iPLEDs. After being modified with an EA layer, the leakage current density curve is shifted upward, yet the leakage current overall remains low (5.7×10^{-6} mA/cm^2 at 1.5 V; Fig. 3A). The current density–luminance–driving voltage characteristic curves (*J*/*L*-*V*), normalized electroluminescence and photoluminescence spectra, and current efficiency–EQE–current density characteristic curves (CE/EQE-J) of a typical nanoscaffold iPLED using SY as the light-emitting material are portrayed in Fig. 3 (B to D). Light emission in this device turns on at 1.8 V and reaches a peak brightness of 2300 cd/m^2 (measured from the anode side) at 18 V. This efficiency is comparable to that of standard sandwich-like iPLEDs (*16*, *23*). Our device (active area of 8 mm^2) can be driven to 10, 200, and 500 cd/m^2 at 6, 12, and 14 V, respectively. Because of the thicker light-emitting layer (300 nm) and unbalanced charge injection, these voltages are slightly higher than those of ordinary polymer iPLED (*17*, *24*, *25*). When the device was turned on, the yellow light generated within the patterned pixel was viewed (Fig. 3B, inset), and the electroluminescence spectra of the yellow were recorded (Fig. 3C). The emission peak of iPLED is located at 560 nm with a full width at half maximum of 74 nm. Here, the average current efficiency of 0.7 cd/A and an EQE of 0.2% were achieved for the SY-based nanoscaffold iPLED (Fig. 3D).

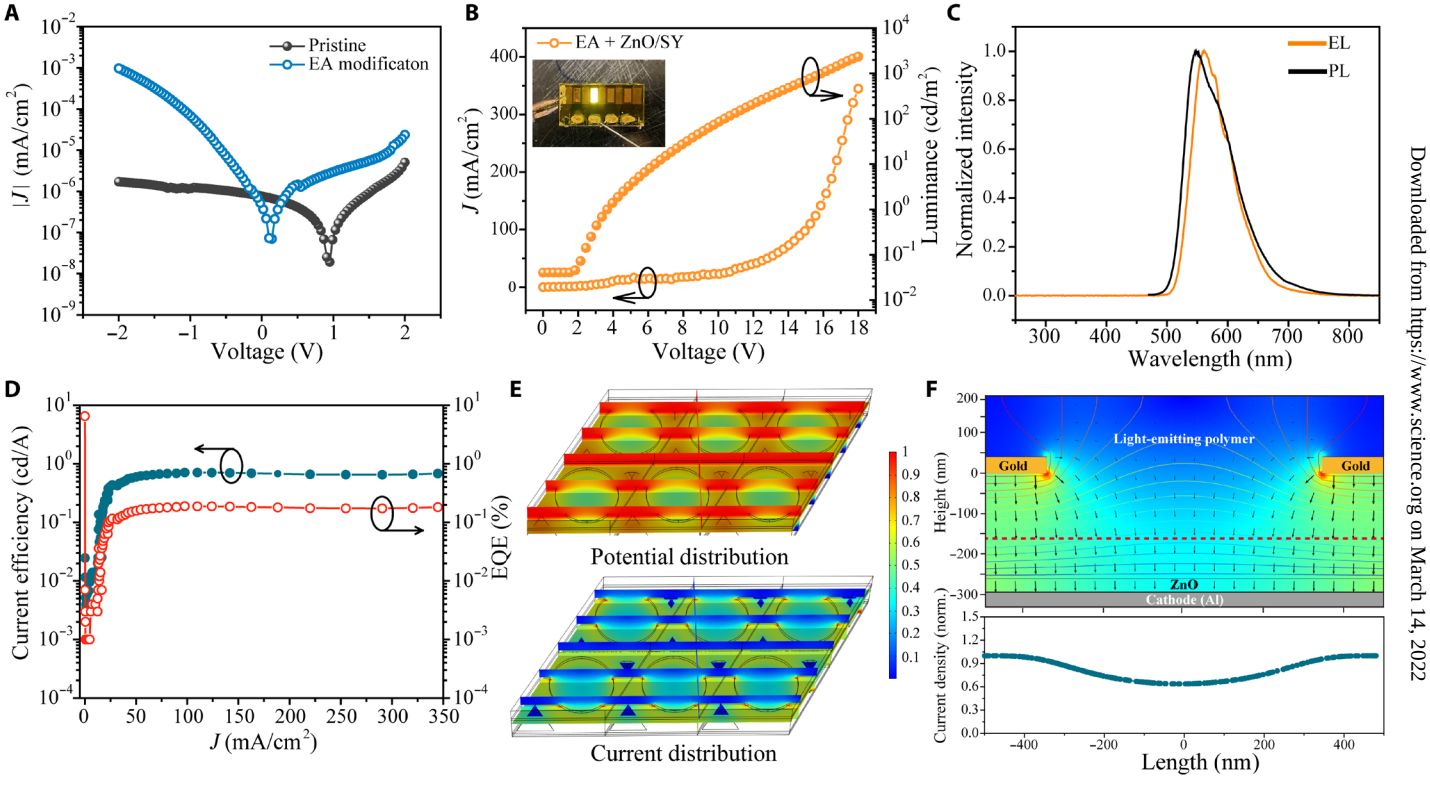

Fig. 3. Device characterization of vertical nanoscaffold iPLEDs. (**A**) *J*-*V* curves of an empty vertical nanoscaffold on the rigid glass substrate before and after EA modification. (**B**) Current density–luminance–driving voltage characteristics of a vertical nanoscaffold iPLED with EA modification. Inset: Photograph of the iPLED (emission area, 2.0 mm by 4.0 mm) biased at 16 V. (**C**) Normalized photoluminescence (PL) and electroluminescence (EL) spectra of the iPLED. (**D**) Current efficiency (cd/A) and EQE characteristics versus current density (mA/cm^2). (**E**) Simulated 3D potential and current distribution in the vertical nanoscaffold iPLED. (**F**) Cross section (front view) of the nanoscaffold device. The top shows finite-element simulations using biasing conditions ($V = -20$ V) that account for the distributions of current density and electric potential within the active cell of the nanoscaffold iPLED. The simulations were performed by considering a nanomesh electrode with 680-nm perforation gaps and 260-nm PI-nanopyramid spacer. For all architectures, the solutions are plotted along with the light-emitting polymer layer. The current density distributions are represented by arrows, while the electric potentials are visualized by the color scale (provided at the left-hand side). The solid lines are equipotential. The bottom displays the horizontal components of the current density near the gold nanomesh, with the profile red dotted lines being exhibited at the top of the panel.

Figure S13 displays the efficiency of a nanoscaffold iPLED without EA modification as the control experiment. The nanoscaffold iPLED without EA modification exhibits a larger current density, inferior luminance, and lower device stability when compared to the device with EA modification. The interfacial negative dipole effect, which is formed spontaneously by the absorption of the amine and hydroxyl groups of EA on ZnO, can minimize the contact barrier between the active polymer and the ZnO when the ZnO surface is treated with a polar solvent (*26*). Similarly, the device has a higher stability after modification with EA when working under a constant current (see fig. S14). Because of the unique vertical-yet-open architecture, the dry transfer approach was used to selectively modify the anode (gold nanomesh) following EA spin coating (see fig. S15). Although we have explored different hole injection materials and thicknesses, such as poly(3,4-ethylenedioxythiophene):poly(styrenesulfonic acid) and MoO_3 (thickness: 1 to 20 nm), we were unable to selectively modify the anode, as displayed in the AFM image in fig. S15B. Furthermore, the iPLEDs performed poorly compared to those without anode modification, likely due to PDMS contamination or nonuniform film transfer. We have also prepared the nanoscaffold iPLEDs with smaller nanopores (diameter: ~260 nm), which showed a substantially higher leakage current density (~ 2 mA/cm^2 at 1.5 V), leading to steep current densities and unsteady brightness in its devices. Furthermore, the small nanopores are extremely brittle; for example, after 2 min of sonication in toluene, the majority of gold nanoelectrodes were ripped away from the substrate (see fig. S16). We think that there are several factors resulting to the relatively low EQE performance: First is the unbalanced charge injection. Because of the vertical device architecture, we can hardly selectively modify the anode as a result of the unbalanced hole/electron injection and transport. Second is the thick coating of light-emitting material. The PI supporting layer determines the thickness of the light-emitting layer, as a result of a very thick light-emitting layer and high operating voltage. Third is the current leakage, especially at high voltage. Under high voltage (>10 V), the lack of insulation of thousands of individual PI pillars could result in a large leakage current.

To corroborate the experimental results, finite element calculations based on COMSOL simulations have been carried out. As in the experiments, the nanoscaffold iPLED device comprised five stacked layers. Both 3D modeling (containing six nanopores) and 2D cross section of a single active cell have been simulated (Fig. 3, E and F) with perforation gaps (i.e., sized pores) of 680 nm while the devices were biased at −20 V (*27*). Figure 3E shows the 3D potential and current density distributions inside six active cells, while the normalized color scale corresponds to the electric potential and current. Figure 3F displays the current distributions (indicated with arrows) within a single active cell, while the color gradient corresponds to the electric potential. In the case of a 680-nm perforation gap, charges are injected into the gap by the vertical electric fields, which are projected by the gold nanomesh edges. The current density distribution is concentrated in the vicinities of the gold nanomesh edges and slightly reduced in the center of the perforation gap (as evident in the bottom of Fig. 3F), indicating that light can be directly emitted from the nanopores, but its intensity may slightly decrease at the center.

Photolithography patterning and recycling of vertical nanoscaffold iPLEDs

As a proof of concept, well-defined micropatterns (from ~500 to ~10 μm) were successfully created in the vertical nanoscaffold using conventional photolithography, and corresponding micropatterned nanoscaffold iPLEDs were fabricated by spin coating of SY. Figure 4A (left) shows dark mode optical microscopy pictures of patterned nanoscaffold iPLED with SY as the light-emitting material. It reveals

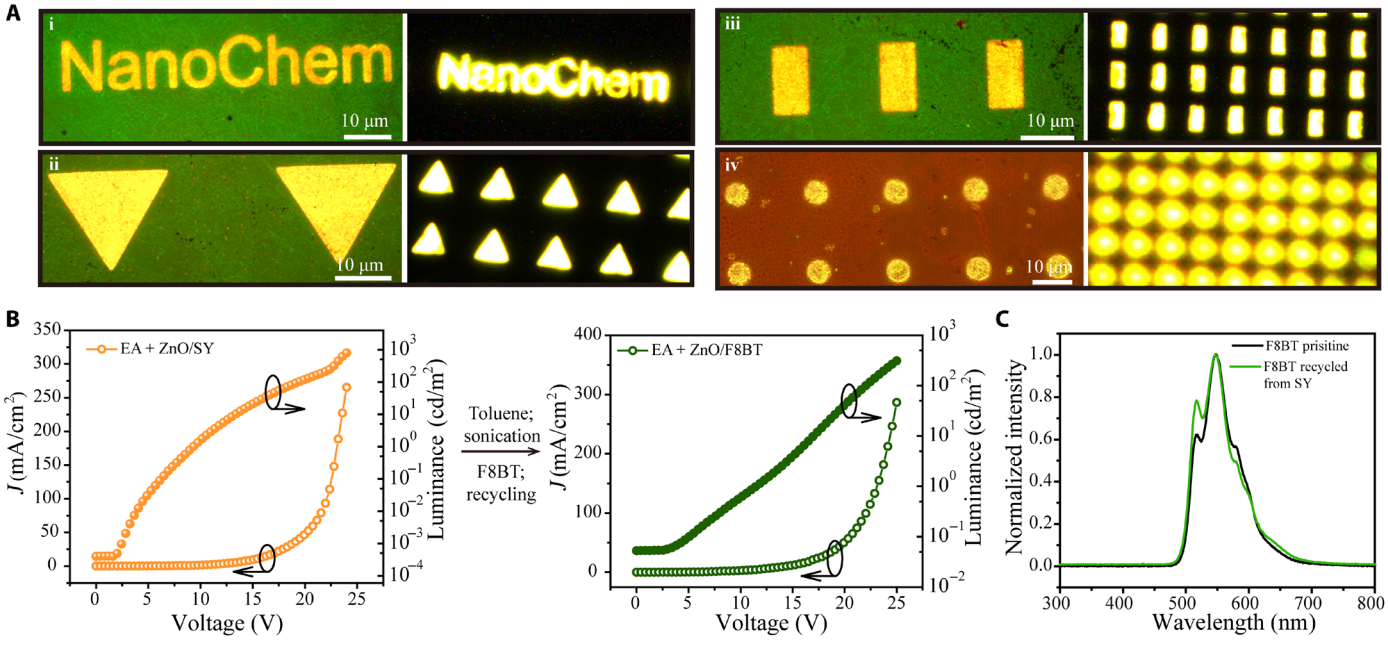

Fig. 4. Micropatterning and recycling of vertical nanoscaffold iPLEDs. (**A**) Dark-field optical microscopy images of micropatterned nanoscaffold iPLEDs prepared by photolithography (left). Electroluminescent photos of micropatterned nanoscaffold iPLEDs under operation (right). (**B**) Current density–luminance–driving voltage characteristics of an old iPLED (left: SY as the light-emitting layer) and its corresponding recycled new iPLED after toluene cleaning (right: F8BT as the light-emitting layer). (**C**) Comparison of electroluminescence spectra of pristine F8BT nanoscaffold iPLED and reused F8BT iPLED from an old SY device.

well-resolved micropatterns with distinct and sharp edges. Significantly, the pixel size in the pattern made with the vertical nanoscaffold iPLED is defined by the nanopore size, which is ~680 nm. Figure 4A (right) shows optical microscopy images of the micropatterned nanoscaffold iPLED in action.

As shown earlier, the vertical nanoscaffold has an excellent structural and mechanical resilience when exposed to a variety of severe environments, which allows iPLEDs to be washed from a given emitting layer and reused once refilled with a new one. Figure 4B shows standard current density–luminance–driving voltage characteristic curves (*J*/*L*-*V*) of an old SY nanoscaffold device, with a turn-on voltage at 2.0 V and a peak brightness of 1000 cd/m^2. The light-emitting polymer SY can be completely removed upon sonication in toluene, as shown by fluorescence microscopy (fig. S17). Subsequently, the incorporation of the polished nanoscaffolds with F8BT ink enables yield green-emitting devices upon recycling an iPLED previously emitting yellow light. The current density–luminance–driving voltage characteristic curves (*J*/*L*-*V*) for the F8BT-based nanoscaffold iPLED were likewise evident, with a turn-on voltage at 2.5 V and a peak brightness of 311 cd/m^2. The output emission peaks of the freshly fabricated and reused F8BT iPLEDs are identical at 547 nm (Fig. 4C and fig. S18), confirming that the SY was completely washed away with no residue. This demonstration, which involves the recycling an outdated nanoscaffold iPLED, demonstrates the enormous potential of our technique to reconditioning display screens and light-emitting materials containing abundant rare earth elements, being of crucial importance for future sustainable developments.

Brush coating and flexible nanoscaffold display

The vertical nanoscaffold, in view of its uniquely designed 3D nanopores, is compatible with a wide variety of solution-processing techniques, like drop casting, spin and spray coating, inkjet printing, and unconventional brush coating. Brush coating is a newly emerging liquid-phase deposition technology that holds a great potential for application in cutting-edge organic optoelectronic devices (*28*, *29*). During the brush processing, the solution may maintain a dynamic balance with the quasi-paralleled conical fibers in the Chinese brush, resulting in the formation of a uniform film (*30*, *31*). As the Chinese brush scans across the substrate surface, the solution on the brush is steadily transferred onto the substrate, forming a liquid thin film as shown in Fig. 5A. By applying such a brush coating on the vertical nanoscaffold pixels, a highly uniform film is generated in each individual nanopore. We have painted with the SY ink eight different arbitrary patterns such as vertical/horizontal lines, square, and numbers (Fig. 5B). The electroluminescent images of brush-coated nanoscaffold iPLEDs in actions are displayed in Fig. 5C. They reveal that it is possible to easily customize a display screen by painting and drawing and that such a device can be reused multiple times.

Significantly, the vertical nanoscaffolds can also be supported on flexible substrates such as PI foil (fig. S19). Figure 5D shows the empty nanoscaffold devices on a flexible PI substrate: Because of its minuscule weight, it can be propped up by a single hair. After being delaminated from the glass support, the background leakage current density of the nanoscaffold on flexible PI displays virtually identical values to those observed when supported on rigid substrate (Fig. 5E). The empty nanoscaffold robustness was explored by performing bending fatigue tests, as shown in Fig. 5F and fig. S20. SEM images showed that the morphology and structure of the nanoscaffold are unaltered after the bending tests (fig. S21). Furthermore, the background ultralow leakage current density remains constant after 1000 bending cycles, providing unambiguous evidence for the notably high robustness of our vertical nanoscaffold. Even if the device is drilled by a needle, it can still work without exhibiting short circuits (fig. S22). The mechanical stability of flexible the nanoscaffold iPLEDs was also examined in a nitrogen-filled glovebox. The current density, luminescence, and driving voltage characteristics of nanoscaffold iPLEDs before and after 1000 folding events are shown in Fig. 5G. The flexible nanoscaffold iPLED showed a

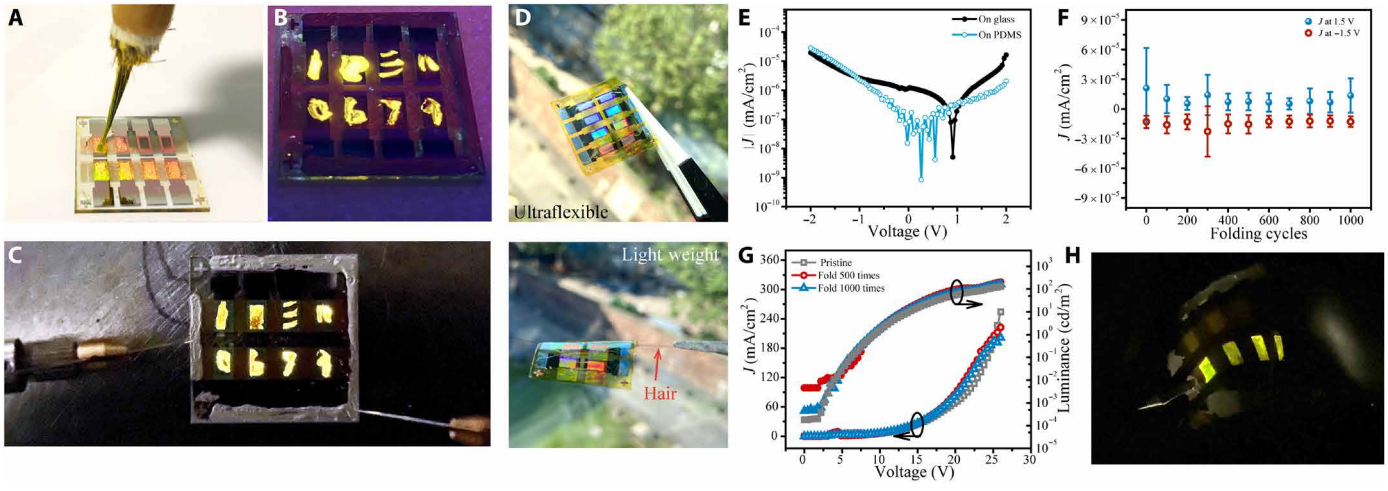

Fig. 5. Brush-painted iPLEDs and flexible nanoscaffold display. (**A**) Photograph of the brush coating process where the light-emitting polymer solution was homogeneously drawn onto the device. (**B**) Photograph of brush-patterned nanoscaffold iPLEDs under 365-nm ultraviolet light irradiation. (**C**) Electroluminescent image of nanoscaffold iPLED display. The patterns were created through brush coating (top: one vertical line, square, three horizontal lines, and two sloping lines; bottom: numbers 0, 6, 7, and 9). (**D**) Images of empty vertical nanoscaffolds on free-standing flexible PI substrate. (**E**) *J*-*V* curves of an empty nanoscaffold on flexible PI before and after delamination from glass. (**F**) The vertical nanoscaffold on the flexible PI substrate retains its characteristics when subjected to >1000 folding events as evidenced by an unchanged leakage current density. (**G**) Current density–luminance–driving voltage characteristics of a nanoscaffold iPLED before and after folding >1000 times. (**H**) Demonstrations of flexible nanoscaffold iPLED display being folded (pixel size, 2 mm × 4 mm). [The size of glass and PI foils in (A) to (D) is 2.5 cm by 2.5 cm].

luminance of 200 cd/m^2 at 26 V at the initial state. The current density decreased 20% when bended >1000 times at a bending radius of 1.5 mm, which can be explained by the generation of cracks in the scaffold. Furthermore, taking full advantage of the nanoscaffold iPLED, a monolithic array of iPLEDs consisting of 4 pixels was fabricated by means of the same technique. Last, Fig. 5H shows a freestanding pixel array in its "on" state when bended, with all pixels being illuminated.

DISCUSSION

We have devised an unprecedented device configuration with a flexible but robust asymmetric vertical-yet-open nanoscaffold as an alternative architecture to replace the conventional sandwich-like structured OLEDs. The vertical nanoscaffold technique can overcome most of the current limitations existing in solution-processed organic light-emitting devices, like pinholes and short circuits. The vertical nanoscaffold is also compatible with conventional photolithography; thus, it can represent a cornerstone in solution-processed ultrahigh-resolution display technology. As an alternative to ITO, patterned aluminum and ZnO are used as the bottom cathode to effectively enhance electron injection from the electrode to the organic layers. The vertical nanoscaffold is extremely reliable: 96% of the ~400 devices displayed negligible leakage currents. The light-emitting polymer SY was deposited by spin coating and brush painting with a pixel resolution as high as 10 μm and a "drop-on-demand" capability, indicating that our nanoscaffold can have a significant impact on the development of high-resolution OLED displays and will open new perspectives on the fabrication of submicrometer vertical organic optoelectronic devices (*32*). Taking advantage of their superior mechanical and structural stability of the nanoscaffold, the used devices can be recycled into new ones with the capability of varying the emitting color, and upon recuperating the original light-emitting material. Foldable devices based on vertical nanoscaffold with state-of-the-art performance were successfully fabricated using PI foil as support, endowing enhanced mechanical flexibility to the architecture. It is also worth noting that the complexity of device processing may limit this technology from being used for display panels.

The relevance of our 3D vertical nanoscaffolds for high-performance optoelectronics applications goes well beyond light-emitting devices and can be tailored for the fabrication of high-performance solar cells, vertical transistors, and sensors (*33*–*36*), as well as electronic wallpapers, rollable screens, and indoor or outdoor luminous advertisement boards. In the future, the replacement of PI with a thinner high-κ dielectrical layer (Al_2O_3 or HfO_2) shall lead to even better device performance, for example, attaining higher luminance and EQE and lower driving voltage. Furthermore, a wider variety of light-emitting materials, such as thermally activated delayed fluorescence material quantum dots (*37*, *38*) and hybrids thereof, may be compatible with our system. Our robust vertical self-suspended nanoscaffold is a powerful device architecture that can fully exploit the unique features of organic semiconducting materials, offering a major step forward in the field of OLEDs and, more generally, in flexible optoelectronics.

MATERIALS AND METHODS

Materials

The monodispersed suspension of PS nanospheres [10 weight % (wt %) in water], SY light-emitting poly (1,4-phenylene vinylene) copolymer, F8BT [weight-average molecular weight (M_w) ≤ 25,000], zinc acetate dihydrate (99.999%), 2-methoxyethanol (99%), poly(sodium-4-styrenesulfonate) solution (PSSNa; M_w ~ 200,000, 30 wt % in H_2O), PMMA (average M_w ~ 350,000), and poly(pyromellitic dianhydride-*co*-4,4′-oxydianiline), amic acid solution (PAA) (11 ± 5 wt %) were purchased from Sigma-Aldrich without further purification. EA (>99%) and *N*,*N*-dimethylacetamide (DMAC) (>99%) were purchased from Tokyo Chemical Industry Co., Ltd. (TCI) Chemicals without further purification. The ultra-flat quartz– coated glass was purchased from Ossila (with the size of 25 mm by 25 mm).

Substrate preparation

Glass substrates were completely cleaned and dried in a nitrogen flow of high purity. The bottom Al electrode (40 nm) was deposited onto the substrate through thermal evaporation. A 0.75 M ZnO solution was synthesized by dissolving zinc acetate dehydrate [$Zn(CH_3COO)_2$ $2H_2O$] in 2-methoxyethanol and EA cosolvents. This solution was stirred at 80°C for 30 min to yield a clear and homogeneous solution (*26*, *39*). The ZnO precursor solution was spin-coated onto cleaned glass substrates patterned with Al electrodes and then placed on a hotplate with a temperature up to 300°C. After that, PAA [in the DMAC solution; PAA:DMAC: 1:2 (v/v)] was deposited by spin coating at 1500 rpm, forming a film with the thickness of 260 nm. Thermal annealing at 140°C of 1 hour was used to remove the solvent residue before 300°C thermal cross-linking treatment of the PI dielectric layer in the glovebox (*40*). The PI thickness is easy to tune by preparing PAA solution in different concentrations when a fixed spin rate was used.

Nanoscaffold preparation

The 40-nm Au nanomesh electrode was nanopatterned on top of the 260-nm layer of PI by nanosphere lithography using the method described in the literature (*18*, *41*). A protective layer of 0.8-nm Cr was placed between the Au and the PI. Then, traditional photolithography step was processed as the mask to define the device surface (2 mm by 4 mm). Subsequently, Cr etchant was used to remove the 0.8-nm Cr protective layer. Last, using oxygen plasma, the areas of the PI dielectric layer that were not protected by photoresist would be removed under a 100-W plasma treatment.

iPLED cell fabrication and characterization

The EA/2-methoxyethanol [1:20 (v/v)] was spin-coated onto vertical nanoscaffold at 3000 rpm and dried for 10 min at 120°C. The emissive layer of SY or F8BT (dichlorobenzene; 10 mg/ml) was then spin-coated onto the vertical nanoscaffold modified with a thin EA layer and annealed at 170°C for 30 min in the glovebox. Last, PMMA (60 mg/ml) from *n*-butyl acetate was spin-coated on the emissive layer as the encapsulation layer and annealed at 90°C for 30 min in the glovebox. The area of the device amounted to 8.0 mm^2. KPFM imaging was performed with a Bruker Dimension Icon AFM. SP images were collected with Pt/Ir-coated silicon probes (Bruker SCM-PIT-V2; resonant frequency ≈ 75 kHz, $k \approx 3$ N m^{-1}) at ambient conditions in the amplitude modulation mode. The *J*/*L*-*V* characteristics and efficiencies were measured using a Keithley 2636A Source Meter, and the irradiation intensity of the devices was measured by a photodiode (Hamamatsu S3204-08), which has been previously calibrated by a luminance meter (Konica Minolta, LS-100) (*42*, *43*).

Recycling of vertical nanoscaffold iPLEDs

The old nanoscaffold iPLEDs can be reused via their ultrasonication cleaning in toluene. The toluene can wash away the deposited PMMA, light-emitting polymer, and EA, resulting in an empty vertical nanoscaffold after 5 min of sonication. The recleaned empty nanoscaffold can then be refilled to obtain a new iPLED through solution processing new light-emitting materials into it.

Nanoscaffold-based flexible display preparation

PSSNa was diluted [1:2 (v/v)] in deionized water, degassed for 5 min, and filtered through a 0.45-μm pore size nylon filter before being spin-coated at 1500 rpm for 30 s on a clean ultra-flat glass previously treated with plasma oxygen (*44*, *45*). The PSSNa layer was annealed for 30 min at 150°C in air as the sacrificial layer. Prepolymer PAA (11 ± 5 wt %) was coated on a PSSNa-modified glass at of 2000 rpm for 50 s without dilution and then annealed at 140° and 300°C in air. For the flexible devices, the polymerized PI layer was used as a supporting layer. Nanoscaffold was then prepared using the method described above.

Theoretical modeling

The finite-element simulations were performed in COMSOL Multiphysics. A 2D space coupled to the quasi-statics electric model was used to simulate in-plane electric currents in the vertical nanoscaffold structures. The calculations were done along a representative device cross section composed of cathode (Al), electron transport layer (ZnO), nanopyramid dielectric (PI), light-emitting polymer (SY), and anode (Au) from the bottom to the top of the nanoscaffold iPLED, respectively. The thickness of the Al, ZnO, PI-nanopyramid spacers, and Au nanomesh are defined as 40, 36, 260, and 40 nm, respectively. The electrical properties, such as conductivity (σ) of the electrodes, were given by the software library. For the light-emitting layer and electron transport layer, we have used $\sigma_{SY} \sim 10^{-11}$ S/cm (*46*) and $\sigma_{ZnO} \sim 10^{-7}$ S/cm (*47*). To complete the simulation, the driving voltage was set to $V = -20$ V and the cathode electrode being grounded, based on the experimental data collected during the device operation.

SUPPLEMENTARY MATERIALS

Supplementary material for this article is available at https://science.org/doi/10.1126/sciadv.abn2225

REFERENCES AND NOTES

1. J. Liang, L. Li, X. Niu, Z. Yu, Q. Pei, Elastomeric polymer light-emitting devices and displays. *Nat. Photonics* **7**, 817–824 (2013).
2. M. S. White, M. Kaltenbrunner, E. D. Glowacki, K. Gutnichenko, G. Kettlgruber, I. Graz, S. Aazou, C. Ulbricht, D. A. M. Egbe, M. C. Miron, Z. Major, M. C. Scharber, T. Sekitani, T. Someya, S. Bauer, N. S. Sariciftci, Ultrathin, highly flexible and stretchable PLEDs. *Nat. Photonics* **7**, 811–816 (2013).
3. T. Yokota, P. Zalar, M. Kaltenbrunner, H. Jinno, N. Matsuhisa, H. Kitanosako, Y. Tachibana, W. Yukita, M. Koizumi, T. Someya, Ultraflexible organic photonic skin. *Sci. Adv.* **2**, e1501856 (2016).
4. L. Hou, X. Zhang, G. F. Cotella, G. Carnicella, M. Herder, B. M. Schmidt, M. Pätzel, S. Hecht, F. Cacialli, P. Samorì, Optically switchable organic light-emitting transistors. *Nat. Nanotechnol.* **14**, 347–353 (2019).
5. OLED Market with COVID-19 Impact Analysis by Product Type (Smartphones, Television Sets, Smart Wearables, Large Format Displays), Panel Type, Panel Size, Technology, Vertical, and Geography - Global Forecast to 2026. (ResearchAndMarkets, 2021).
6. M. Y. Wong, E. Zysman-Colman, Purely Organic Thermally Activated Delayed Fluorescence Materials for Organic Light-Emitting Diodes. *Adv. Mater.* **29**, 1605444 (2017).
7. R. Visbal, M. C. Gimeno, N-heterocyclic carbene metal complexes: Photoluminescence and applications. *Chem. Soc. Rev.* **43**, 3551–3574 (2014).
8. Z. Cheng, Y. Wang, D. M. O'Carroll, Influence of partially-oxidized silver back electrodes on the electrical properties and stability of organic semiconductor diodes. *Org. Electron* **70**, 179–185 (2019).
9. J. W. Han, B. Jung, D. W. Kim, K. T. Lim, S.-Y. Jeong, Y. H. Kim, Transparent conductive hybrid thin-films based on copper-mesh/conductive polymer for ITO-Free organic light-emitting diodes. *Org. Electron* **73**, 13–17 (2019).
10. V. Bulović, V. B. Khalfin, G. Gu, P. E. Burrows, D. Z. Garbuzov, S. R. Forrest, Weak microcavity effects in organic light-emitting devices. *Phys. Rev. B* **58**, 3730–3740 (1998).
11. A. Chutinan, K. Ishihara, T. Asano, M. Fujita, S. Noda, Theoretical analysis on light-extraction efficiency of organic light-emitting diodes using FDTD and mode-expansion methods. *Org. Electron* **6**, 3–9 (2005).
12. G. Gu, D. Z. Garbuzov, P. E. Burrows, S. Venkatesh, S. R. Forrest, M. E. Thompson, High-external-quantum-efficiency organic light-emitting devices. *Opt. Lett.* **22**, 396–398 (1997).
13. Y. Sun, S. R. Forrest, Enhanced light out-coupling of organic light-emitting devices using embedded low-index grids. *Nat. Photonics* **2**, 483–487 (2008).
14. L. Zhang, X. Zhong, E. Pavlica, S. Li, A. Klekachev, G. Bratina, T. W. Ebbesen, E. Orgiu, P. Samorì, A nanomesh scaffold for supramolecular nanowire optoelectronic devices. *Nat. Nanotechnol.* **11**, 900–906 (2016).
15. L. Zhang, N. Pasthukova, Y. Yao, X. Zhong, E. Pavlica, G. Bratina, E. Orgiu, P. Samorì, Self-Suspended Nanomesh Scaffold for Ultrafast Flexible Photodetectors Based on Organic Semiconducting Crystals. *Adv. Mater.* **30**, 1801181 (2018).
16. D. Kabra, M. H. Song, B. Wenger, R. H. Friend, H. J. Snaith, High efficiency composite metal oxide-polymer electroluminescent devices: A morphological and material based investigation. *Adv. Mater.* **20**, 3447–3452 (2008).
17. B. R. Lee, E. D. Jung, J. S. Park, Y. S. Nam, S. H. Min, B. S. Kim, K. M. Lee, J. R. Jeong, R. H. Friend, J. S. Kim, S. O. Kim, M. H. Song, Highly efficient inverted polymer light-emitting diodes using surface modifications of ZnO layer. *Nat. Commun.* **5**, 4840 (2014).
18. T. C. Gao, B. M. Wang, B. Ding, J. K. Lee, P. W. Leu, Correction to Uniform and Ordered Copper Nanomeshes by Microsphere Lithography for Transparent Electrodes. *Nano Lett.* **14**, 3694–3694 (2014).
19. A. Liscio, E. Orgiu, J. M. Mativetsky, V. Palermo, P. Samorì, Bottom-up fabricated asymmetric electrodes for organic electronics. *Adv. Mater.* **22**, 5018–5023 (2010).
20. T.-W. Lee, O. O. Park, The Effect of Different Heat Treatments on the Luminescence Efficiency of Polymer Light-Emitting Diodes. *Adv. Mater.* **12**, 801–804 (2000).
21. C. Y. Chen, W. K. Lee, Y. J. Chen, C. Y. Lu, H. Y. Lin, C. C. Wu, Enhancing optical out-coupling of organic light-emitting devices with nanostructured composite electrodes consisting of indium tin oxide nanomesh and conducting polymer. *Adv. Mater.* **27**, 4883–4888 (2015).
22. Y. G. Li, M. Kovacic, J. Westphalen, S. Oswald, Z. F. May, C. Hanisch, P. A. Will, L. H. Jiang, M. Junghaehnel, R. Scholz, S. Lenk, S. Reineke, Tailor-made nanostructures bridging chaos and order for highly efficient white organic light-emitting diodes. *Nat. Commun.* **10**, 2972 (2019).
23. H. J. Bolink, E. Coronado, J. Orozco, M. Sessolo, Efficient polymer light-emitting diode using air-stable metal oxides as electrodes. *Adv. Mater.* **21**, 79–82 (2009).
24. H. Fukagawa, T. Sasaki, T. Tsuzuki, Y. Nakajima, T. Takei, G. Motomura, M. Hasegawa, K. Morii, T. Shimizu, Long-lived flexible displays employing efficient and stable inverted organic light-emitting diodes. *Adv. Mater.* **30**, 1706768 (2018).
25. S. Hofle, A. Schienle, C. Bernhard, M. Bruns, U. Lemmer, A. Colsmann, Solution processed, white emitting tandem organic light-emitting diodes with inverted device architecture. *Adv. Mater.* **26**, 5155–5159 (2014).
26. B. R. Lee, E. D. Jung, Y. S. Nam, M. Jung, J. S. Park, S. Lee, H. Choi, S. J. Ko, N. R. Shin, Y. K. Kim, S. O. Kim, J. Y. Kim, H. J. Shin, S. Cho, M. H. Song, Amine-based polar solvent treatment for highly efficient inverted polymer solar cells. *Adv. Mater.* **26**, 494–500 (2014).
27. A. Nawaz, L. Merces, D. M. de Andrade, D. H. S. de Camargo, C. C. B. Bufon, Edge-driven nanomembrane-based vertical organic transistors showing a multi-sensing capability. *Nat. Commun.* **11**, 841 (2020).
28. C. Guo, X. Gao, F. J. Lin, Q. Wang, L. Meng, R. Bian, Y. Sun, L. Jiang, H. Liu, In situ characterization of the triphase contact line in a brush-coating process: Toward the enhanced efficiency of polymer solar cells. *ACS Appl. Mater. Interfaces* **10**, 39448–39454 (2018).
29. X. Zhang, J. An, Y. Xu, Y. Wang, Y. Lu, Y. Qin, W.-Y. Lai, Y. Chen, W. Huang, Efficient small molecule organic light-emitting diodes fabricated by brush-coating. *J. Mater. Chem. C* **9**, 2190–2197 (2021).
30. M. Zhang, B. Hu, L. Meng, R. Bian, S. Wang, Y. Wang, H. Liu, L. Jiang, Ultrasmooth quantum dot micropatterns by a facile controllable liquid-transfer approach: Low-cost fabrication of high-performance QLED. *J. Am. Chem. Soc.* **140**, 8690–8695 (2018).
31. Q. Wang, B. Su, H. Liu, L. Jiang, Chinese brushes: Controllable liquid transfer in ratchet conical hairs. *Adv. Mater.* **26**, 4889–4894 (2014).

32. H. W. Park, K. Y. Choi, J. Shin, B. Kang, H. Hwang, S. Choi, A. Song, J. Kim, H. Kweon, S. Kim, K. B. Chung, B. Kim, K. Cho, S. K. Kwon, Y. H. Kim, M. S. Kang, H. Lee, D. H. Kim, Universal route to impart orthogonality to polymer semiconductors for sub-micrometer tandem electronics. *Adv. Mater.* **31**, e1901400 (2019).
33. J. Lenz, F. del Giudice, F. R. Geisenhof, F. Winterer, R. T. Weitz, Vertical, electrolyte-gated organic transistors show continuous operation in the MA cm(−2) regime and artificial synaptic behaviour. *Nat. Nanotechnol.* **14**, 579–585 (2019).
34. Z. Wu, Y. Liu, E. Guo, G. Darbandy, S. J. Wang, R. Hubner, A. Kloes, H. Kleemann, K. Leo, Efficient and low-voltage vertical organic permeable base light-emitting transistors. *Nat. Mater.* **20**, 1007–1014 (2021).
35. J. Liu, J. Wang, Z. Zhang, F. Molina-Lopez, G. N. Wang, B. C. Schroeder, X. Yan, Y. Zeng, O. Zhao, H. Tran, T. Lei, Y. Lu, Y. X. Wang, J. B. Tok, R. Dauskardt, J. W. Chung, Y. Yun, Z. Bao, Fully stretchable active-matrix organic light-emitting electrochemical cell array. *Nat. Commun.* **11**, 3362 (2020).
36. S. H. Chae, W. J. Yu, J. J. Bae, D. L. Duong, D. Perello, H. Y. Jeong, Q. H. Ta, T. H. Ly, Q. A. Vu, M. Yun, X. F. Duan, Y. H. Lee, Transferred wrinkled Al_2O_3 for highly stretchable and transparent graphene-carbon nanotube transistors. *Nat. Mater.* **12**, 403–409 (2013).
37. Q. Sun, Y. A. Wang, L. S. Li, D. Wang, T. Zhu, J. Xu, C. Yang, Y. Li, Bright, multicoloured light-emitting diodes based on quantum dots. *Nat. Photonics* **1**, 717–722 (2007).
38. Z. Yang, Z. Mao, Z. Xie, Y. Zhang, S. Liu, J. Zhao, J. Xu, Z. Chi, M. P. Aldred, Recent advances in organic thermally activated delayed fluorescence materials. *Chem. Soc. Rev.* **46**, 915–1016 (2017).
39. Y. Sun, J. H. Seo, C. J. Takacs, J. Seifter, A. J. Heeger, Inverted polymer solar cells integrated with a low-temperature-annealed sol-gel-derived ZnO film as an electron transport layer. *Adv. Mater.* **23**, 1679–1683 (2011).
40. D. Ji, X. Xu, L. Jiang, S. Amirjalayer, L. Jiang, Y. Zhen, Y. Zou, Y. Yao, H. Dong, J. Yu, H. Fuchs, W. Hu, Surface polarity and self-structured nanogrooves collaboratively oriented molecular packing for high crystallinity toward efficient charge transport. *J. Am. Chem. Soc.* **139**, 2734–2740 (2017).
41. A. Sinitskii, J. M. Tour, Patterning graphene through the self-assembled templates: Toward periodic two-dimensional graphene nanostructures with semiconductor properties. *J. Am. Chem. Soc.* **132**, 14730–14732 (2010).
42. Y. Chen, H. Wang, Y. Yao, Y. Wang, C. Ma, P. Samori, Synaptic plasticity powering long-afterglow organic light-emitting transistors. *Adv. Mater.* **33**, 2103369 (2021).
43. S. R. Forrest, D. D. C. Bradley, M. E. Thompson, Measuring the efficiency of organic light-emitting devices. *Adv. Mater.* **15**, 1043–1048 (2003).
44. D. Ji, A. D. Donner, G. Wilde, W. Hu, H. Fuchs, Poly(sodium-4-styrene sulfonate) (PSSNa)-assisted transferable flexible, top-contact high-resolution free-standing organic field-effect transistors. *RSC Adv.* **5**, 98288–98292 (2015).
45. F. Molina-Lopez, T. Z. Gao, U. Kraft, C. Zhu, T. Ohlund, R. Pfattner, V. R. Feig, Y. Kim, S. Wang, Y. Yun, Z. Bao, Inkjet-printed stretchable and low voltage synaptic transistor array. *Nat. Commun.* **10**, 2676 (2019).
46. M. M. Szindler, M. Szindler, L. A. Dobrzański, The structure and conductivity of polyelectrolyte based on MEH-PPV and potassium iodide (KI) for dye-sensitized solar cells. *Open Phys.* **15**, 1022–1027 (2017).
47. M. Caglar, S. Ilican, Y. Caglar, F. Yakuphanoglu, Electrical conductivity and optical properties of ZnO nanostructured thin film. *Appl. Surf. Sci.* **255**, 4491–4496 (2009).

Acknowledgments: We thank J. Tan for enlightening discussions. Dedicated to Prof. Fabio Biscarini on the occasion of his 60th birthday. **Funding:** This work was financially supported by the European Union's Horizon 2020 research and innovation programme under the Marie Skłodowska-Curie grant agreement no. 811284 (UHMob) and the ERC Proof of Concept project FlexNanoOLED (GA-766936), the PROSPECT project funded by the FLAG-ERA programme, the Agence Nationale de la Recherche through the Labex project CSC (ANR-10- LABX-0026 CSC) within the Investissement d'Avenir program (ANR-10-120 IDEX-0002-02), the International Center for Frontier Research in Chemistry (icFRC), the Institut Universitaire de France (IUF), and the Chinese Scholarship Council. **Author contributions:** Y.Y., L.Z., and P.S. conceived the experiment. Y.Y. designed the study and fabricated the devices. Y.C. carried out photoluminescence measurements. K.W. performed SEM measurement. Y.Y., Y.C., and H.W. designed and built the device characterization setup. Y.Y. and Y.C. performed the quantitative nanoscaffold iPLED devices characterization. N.T. carried out the KPFM measurements and analysis. S.V. performed pressure stability testing. B.H. carried out the photoelectron spectroscopy measurement. All authors discussed the results and contributed to the interpretation of data. Y.Y. and P.S. co-wrote the paper with input from all co-authors. **Competing interests:** The authors declare that they have no competing interests. **Data and materials availability:** All data needed to evaluate the conclusions in the paper are present in the paper and/or the Supplementary Materials.

Submitted 11 November 2021
Accepted 21 January 2022
Published 11 March 2022
10.1126/sciadv.abn2225

ScienceAdvances

A robust vertical nanoscaffold for recyclable, paintable, and flexible light-emitting devices

Yifan YaoYusheng ChenKuidong WangNicholas TurettaStefania VitaleBin HanHanlin WangLei ZhangPaolo Samorì

Sci. Adv., 8 (10), eabn2225. • DOI: 10.1126/sciadv.abn2225

Science Advances (ISSN) is published by the American Association for the Advancement of Science. 1200 New York Avenue NW, Washington, DC 20005. The title *Science Advances* is a registered trademark of AAAS.